Available online at www.sciencedirect.com
ScienceDirect
Biochimica et Biophysica Acta 1778 (2008) 472–482
Biochimica et Biophysica Acta BBA
www.elsevier.com/locate/bbamem

Insight into the location and dynamics of the annexin A2 N-terminal domain during Ca^{2+}-induced membrane bridging

Jesus Ayala-Sanmartin [a,b,*], Mallik Zibouche [a,b], Françoise Illien [a,b], Michel Vincent [c,d], Jacques Gallay [c,d,*]

[a] *INSERM U538, CHU Saint-Antoine, Paris F-75012, France*
[b] *Université Pierre et Marie Curie, CHU Saint-Antoine, Paris F-75012, France*
[c] *CNRS UMR8619 IBBMC, Orsay F-91405, France*
[d] *Université Paris-Sud, Orsay F-91405, France*

Received 4 June 2007; received in revised form 14 September 2007; accepted 2 November 2007
Available online 17 November 2007

Abstract

Annexin A2 (AnxA2) is a Ca^{2+}- and phospholipid-binding protein involved in many cellular regulatory processes. Like other annexins, it is constituted by two domains: a conserved core, containing the Ca^{2+} binding sites, and a variable N-terminal segment, containing sites for interactions with other protein partners like S100A10 (p11). A wealth of data exists on the structure and dynamics of the core, but little is known about the N-terminal domain especially in the Ca^{2+}-induced membrane-bridging process. To investigate this protein region in the monomeric AnxA2 and in the heterotetramer $(AnxA2\text{-}p11)_2$, the reactive Cys8 residue was specifically labelled with the fluorescent probe acrylodan and the interactions with membranes were studied by steady-state and time-resolved fluorescence. In membrane junctions formed by the $(AnxA2\text{-}p11)_2$ heterotetramer, the flexibility of the N-terminal domain increased as compared to the protein in solution. In "homotypic" membrane junctions formed by monomeric AnxA2, acrylodan moved to a more hydrophobic environment than in the protein in solution and the flexibility of the N-terminal domain also increased. In these junctions, this domain is probably not in close contact with the membrane surface, as suggested by the weak quenching of acrylodan observed with doxyl-PCs, but pairs of N-termini likely interact, as revealed by the excimer-forming probe pyrene-maleimide bound to Cys8. We present a model of monomeric AnxA2 N-terminal domain organization in "homotypic" bridged membranes in the presence of Ca^{2+}.

Keywords: Annexin; N-terminal domain; Acrylodan; Pyrene; Membrane aggregation; Time-resolved fluorescence

1. Introduction

Annexins (Anx) constitute a family of Ca^{2+}-dependent phospholipid-binding proteins with various membrane-related functions [1,2]. These proteins have two domains: a C-terminal core with a conserved structure and a N-terminal domain that is variable in sequence and length [3,4]. The core domain is formed by four repeats (eight for AnxA6) containing Ca^{2+} binding sites [5]. Each repeat consists of five α-helices connected by short loops. The four repeats are organized into a curved oblate shape, with a convex face harbouring the Ca^{2+} binding sites, facilitating contact with the membrane phospholipids. The N-terminal domain, located in the concave face at the opposite of the membrane surface, regulates the membrane-related properties of the core. Modifications of the N-terminal

Abbreviations: Acrylodan, 6-acryloyl-2-dimethylaminonaphthalene; LUV, large unilamellar vesicles; MEM, maximum entropy method; *n*-doxyl PC, 1-palmitoyl-2-stearoyl(*n*-doxyl)-*sn*-glycerophosphatidylcholine ($n=5$, 7 or 12); p11, S100A10 protein; Anx, annexin; $AnxA2^{acryl}$, annexin A2 labelled with acrylodan on Cys8; $AnxA2^{pyr}$, annexin A2 labelled with pyrene on Cys8; $(AnxA2\text{-}p11)_2$, heterotetramer AnxA2-p11; Pyrene-maleimide, *N*-(1-Pyrene) maleimide; PC, egg L-α-glycerophosphatidylcholine; PS, brain L-α-glycerophosphatidyl-L-serine; PE, egg L-α-phosphatidyl-L-ethanolamine; pCa, $-\log [Ca^{2+}]$; L/P, lipid/protein molar ratio

* Corresponding author. Gallay is to be contacted at IBBMC, UMR8619 CNRS Université Paris-Sud Bâtiment 430, F-91405 Orsay, France. Tel.: +33 1 69 15 48 42; fax: +33 1 69 85 37 15. Ayala-Sanmartin is to be contacted at INSERM U538, CHU Saint-Antoine, 27 rue Chaligny, Paris, F-75012 Paris, France. Tel.: +33 1 40 01 13 24; fax: +33 1 40 01 13 90.
E-mail addresses: jayala@chusa.jussieu.fr (J. Ayala-Sanmartin), jacques.gallay@u-psud.fr (J. Gallay).

0005-2736/$ - see front matter © 2007 Elsevier B.V. All rights reserved.
doi:10.1016/j.bbamem.2007.11.004

sequence results in changes in the membrane-binding, aggregation and fusion properties of several annexins [6,7]. Phosphorylation of the N-terminal domain of annexin A1 and mutations mimicking these phosphorylations also modified calcium sensitivity for membrane bridging [8–10]. It has also been suggested that the N-terminal tail of AnxA1 acts as a secondary Ca^{2+}-independent membrane-binding site [11,12].

AnxA2 has been involved in many different membrane processes such as exo- and endocytosis, membrane cytoskeleton organization and blood coagulation [1,2]. The N-terminal tail of the protein (34 residues) is subject to several types of posttranslational modifications, including serine and tyrosine phosphorylation [13–15] N-terminal acetylation [16] and glutathiolation of Cys8 [17]. Signalling role of the N-terminal tail has been described, involving residues 3–12 for nuclear export [18] and its phosphorylation in nuclear import [19]. The N-terminal tail regulates the properties of the AnxA2 core by binding to S100A10 (p11) [20–23], as for AnxA1 and AnxA11, which bind to other members of the S100 family [24–26]. AnxA2 is required for strong binding of S100A10 to the C-terminal domain of the protein AHNAK [27]. These regulatory properties are illustrated by the higher propensity of the heterotetramer $(AnxA2\text{-}p11)_2$ to bind to phospholipid membranes at submicromolar Ca^{2+} concentrations, whereas the monomeric AnxA2 requires micromolar Ca^{2+} concentrations for such binding. Moreover, the phosphorylation of $(AnxA2\text{-}p11)_2$ by protein kinase C decreases the membrane bridging capacity of the protein [14]. Mutants mimicking the phosphorylation of Ser11 and Ser25 displayed modifications of calcium sensitivity for membrane bridging [28,29]. Two proteolytic species of AnxA2, differing in terms of deletions within the N-terminal tail, promote chromaffin granule aggregation, but with different Ca^{2+} sensitivities [30]. Deletion of the N-terminal domain decreases the Ca^{2+} sensitivity of AnxA2 for plasma membrane binding in living cells [31] and in model membranes in vitro [29]. Recently, we showed that dimerization of the protein through the formation of disulfide bridges between Cys8 residues also increased membrane bridging efficiency [32]. The N-terminus of AnxA2 is therefore involved in the regulation of the Ca^{2+}-sensitive membrane bridging by an as yet uncharacterized mechanism.

The three-dimensional structure of the core domain of many annexins has been resolved at the atomic level by X-ray diffraction (see reference [1] for a review). However, little is known about the structure of the N-terminal domains of most annexins and their interactions with the core, with two main exceptions: AnxA1 and AnxA3 [33,34]. The full-length AnxA2 was also crystallized [35] and the structure was resolved except for the first 20 residues [36]. Residues 21 to 33 of the N-terminal tail were shown to be in contact with the concave face of the core. This structure is consistent with the recognition, by monoclonal antibody H28, of an epitope involving residues Arg62, Glu65 and Arg67 of the core and Lys27 of the N-terminal tail [37,38].

Cryo-electron microscopy showed that the respective junctions formed between membranes and heterotetrameric $(AnxA2\text{-}p11)_2$ or monomeric AnxA2, displayed structural differences [39]. Direct interactions between two monomeric AnxA2 molecules via their N-termini-bearing concave faces were in particular proposed to occur in the so-called "homotypic" junctions. In this study, we aimed to investigate these interactions in more detail by steady-state and time-resolved fluorescence spectroscopy, particularly concerning the conformational dynamics of the N-terminal domain of monomeric AnxA2 and heterotetrameric $(AnxA2\text{-}p11)_2$ in their soluble forms and in Ca^{2+}-induced membrane bridging. For this purpose, we specifically labelled the N-terminal segment of AnxA2 by acrylodan, a polarity-sensitive probe, on the only reactive cysteine residue Cys8 [40,41]. This specific labelling has been previously used to study the change in environment of the N-terminal segment during the formation of the (AnxA2-p11)2 heterotetramer [16,21]. The conformational dynamics of the N-terminal segment, in solution or in the Ca^{2+}-induced membrane-bridging state, was however not investigated in this previous study, either in the AnxA2 monomer or in the $(AnxA2\text{-}p11)_2$ heterotetramer. Moreover, we also used the thiol-reactive probe pyrene-maleimide, which can form excimers when two aromatic rings come into sufficiently close contact (<10 Å [42]), to label the same reactive Cys8, which enables to investigate the possible existence of N-terminal interactions between AnxA2 monomers on the membrane surface in the "homotypic" membrane junctions. We propose a model of Ca^{2+}-induced membrane bridging by the monomeric protein in which the N-terminal domains of two adjacent AnxA2 molecules can interact with each other to stabilize the membrane junction.

2. Materials and methods

2.1. Chemicals

Acrylodan and *N*-(1-pyrene) maleimide were purchased from Molecular Probes (Invitrogen, France). Type III-B egg L-α-phosphatidylcholine (PC), brain L-α-phosphatidyl-L-serine (PS), egg L-α-phosphatidyl-L-ethanolamine (PE) and cholesterol were obtained from Sigma-Aldrich, France. Dr. Claude Wolf (CHU Saint-Antoine, Paris) kindly provided distearoyl PC labelled with a doxyl group at positions $n=5$, 7 and 12 of the sn2 chain.

2.2. Protein preparation and labelling with acrylodan and pyrene maleimide

AnxA2 produced in *S. cerevisiae* and p11 produced in *E. coli* were purified as previously described [28]. Protein purity was estimated as >95% as judged by gel electrophoresis. $(AnxA2\text{-}p11)_2$ was obtained by mixing equimolar quantities of AnxA2 and p11. The only reactive cysteine of AnxA2, Cys8, was labelled with acrylodan, as described by Johnsson et al. [21]. Briefly, 1.8 mg of DTT-free purified AnxA2 was incubated with acrylodan at an acrylodan/AnxA2 molar ratio of 2. After 1 h of incubation on ice, the reaction was stopped by adding dithiothreitol (DTT) to a final concentration of 2 mM. The unbound acrylodan was washed out by gel filtration on an Econo-pac 10DG column (Biorad). The protein was concentrated by centrifugation through a Centricon 10 (Whatman), to obtain a 1.6 mg/ml solution of labelled protein. The efficiency of acrylodan labelling was 50%, as estimated using molar extinction coefficients for acrylodan of 16,400 and 6200 M^{-1} cm^{-1} at 385 and 290 nm, respectively [41]. DTT-free AnxA2 was labelled with pyrene-maleimide on its Cys8 residue by incubating 300 μg of purified AnxA2 in 800 μl of PBS (~10 μM protein) with 100 μl of 1.6 mM *N*-(1-pyrene) maleimide in dimethylformamide (final pyrene-maleimide concentration of about 150 μM). After 3 h of incubation in the dark at room temperature, the reaction was stopped by adding DTT to a final concentration of 2 mM. The unbound pyrene-maleimide was washed out by gel filtration on an Econo-pac 10DG column. The protein was concentrated with a Centricon 10, to obtain a 0.4 mg/ml solution of labelled protein. The efficiency of pyrene-

maleimide labelling was 83%, as shown using a molar extinction coefficient at 340 nm of 40,000 M^{-1} cm^{-1} [43]. Labelled proteins were sampled and stored at −20 °C. No alteration of membrane aggregative properties of the labelled protein were observed compared to the unlabelled protein.

2.3. LUV preparation and aggregation

Large unilamellar vesicles (LUVs) with different lipidic compositions, including some mimicking that of the inner leaflet of the plasma membrane, were prepared by extrusion. The lipid mixtures were: PC/PS (75/25 weight ratio); PC/PS/Chl (50/25/25); PC/PS/PE (25/15/60); PC/PS/PE/Chl (20/20/35/25) and PC/PS/PE/Chl (17/12/52/19), this last one being similar to that of natural plasma membrane inner leaflet. Lipids were mixed together in chloroform. The solvent was removed from the mixture under a stream of nitrogen and residual solvent was eliminated under vacuum for 1 h. Lipids were then resuspended to a concentration of 1 mg ml^{-1}, by vortexing vigorously in buffer (40 mM Hepes pH 7, 30 mM KCl, 1 mM EGTA). The multilamellar liposomes were then extruded by passing the suspension 21 times through a polycarbonate membrane with 0.1 μm pores (Avestin, Canada). Free calcium concentration, expressed as pCa (−log [Ca^{2+}]), was controlled by EGTA buffering and vesicle aggregation was monitored by turbidimetry at 340 nm, as previously described [44].

2.4. Steady-state fluorescence measurements

Fluorescence emission spectra were recorded with a Cary Eclipse spectrofluorimeter with slit width of 10 nm and 5 nm for excitation and emission, respectively. Samples were contained in microcuvettes (120 μl).

2.5. Time-resolved fluorescence measurements

Fluorescence intensity and anisotropy decays were calculated from the polarized $I_{vv}(t)$ and $I_{vh}(t)$ components measured by the time-correlated single-photon counting technique. A diode laser (LDH 405 from Picoquant, Berlin-Adlershof, Germany; maximal emission at 392 nm) operating at 10 MHz was used as an excitation source. A Hamamatsu fast photomultiplier (model R3235-01) was used for detection. Emission wavelength was selected with a Jobin–Yvon H10 monochromator (band width 16 nm) and a Schott KV418 cut-off filter. Each experimental decay $I_{vv}(t)$ and $I_{vh}(t)$ was stored on a 2 K plug-in multichannel analyzer card (Ortec Trump-PCI 2k, Ametek France), using Maestro-32 software. Automatic data sampling was controlled by the microcomputer. The instrumental response function (FWHM ~600 ps) was automatically collected by measuring the light scattering of a glycogen solution during 30 s at the excitation wavelength, in alternation with the parallel and perpendicular components of polarized fluorescence decay, each over a total of 90 s. Samples were contained in microcuvettes (120 μl).

Fluorescence intensity decay analyses were performed with MEM, using a multiexponential model: $\sum_i \alpha_i \exp(-t/\tau_i)$, as previously described [45,46]. A classical anisotrophy model: $\sum_i \beta_i \exp(-t/\theta_i)$, in which any rotational correlation time (θ) is coupled with each lifetime (τ), was used to resolve polarized fluorescence decays [47]. Calculations were carried out with a set of 150 or 100 independent variables (equally spaced on a logarithmic scale) for intensity and anisotropy, respectively. The programs, including the MEMSYS 5 subroutines (MEDC Ltd, Cambridge, UK), were written in double-precision FORTRAN 77.

2.6. Fluorescence quenching by iodide and doxyl-PCs

Fluorescence was quenched with iodide, using a solution of 5 M KI in water supplemented with 0.1 mM $Na_2S_2O_3$ to prevent oxidation. Quenching was analyzed using the Stern–Volmer equation: $F_0/F = 1 + K_{SV}[Q]$ where F_0 and F are the fluorescence intensities in the absence and presence of quencher at concentration [Q], respectively; K_{SV} is the Stern–Volmer quenching constant. K_{SV} is related to the bimolecular quenching constant k_q as follows: $K_{SV} = k_q\tau$, where τ is the lifetime in the absence of quencher.

Quenching by doxyl-PCs (labelled at C5, C7 and C12 on the sn2 acyl chain) was carried out with LUV prepared with 10, 20 or 30% molar fractions of labelled PC, 25% PS and supplemented with unlabelled PC.

3. Results

3.1. Conformational dynamics of the AnxA2 N-terminal segment in solution

The steady-state fluorescence emission spectrum of $AnxA2^{acryl}$ peaked at 515–520 nm (Fig. 1) in agreement with the previously reported values [21], confirming that the environment of acrylodan bound to Cys8 in the N-terminal segment is highly polar even in the presence of mM Ca^{2+} concentration (Fig. 1). The high quenching efficiency of iodide, shown by the previously published value of the iodide Stern–Volmer constant (K_{SV} = 2.95 M^{-1}) [21], was confirmed by our measurements (K_{SV} = 2.73 M^{-1}) (Fig. 2 and Table 1). In presence of 2 mM Ca^{2+}, this value was only slightly modified (K_{SV} = 2.98 M^{-1}) (Table 1). It is to be remarked, however, that the use of these K_{SV} values for the estimation of the accessibility to the solvent is valid only if the excited state lifetime values τ are measured. The lifetime values measured in the present work (1.88 ns with and without Ca^{2+}, Table 1) allow calculation of the bimolecular quenching constant k_q values ($k_q = K_{SV}/\langle\tau\rangle$, where $\langle\tau\rangle$ is the amplitude-average lifetime). They are of the order of magnitude of diffusional processes both in the presence or absence of Ca^{2+}, demonstrating the large accessibility of acrylodan to the solvent in both cases (Table 1).

In line with the absence of effect of Ca^{2+} on the acrylodan fluorescence emission spectrum and iodide quenching, the fluorescence intensity decays of $AnxA2^{acryl}$, which is a sensitive tool for local conformational changes, could not be distinguished in the presence and absence of Ca^{2+} (Fig. 3 curves 2 and 3). Both decays were not monoexponential. MEM analysis of the data showed the presence of three lifetime populations (Fig. 4A), probably attributable to the existence of three local conformers since no signature of excited-state reaction could be detected, such as fluorescence build-up at long emission wavelength (data not shown). The center value and amplitude of each lifetime peak (Table 2) were similar in the presence and absence of Ca^{2+}.

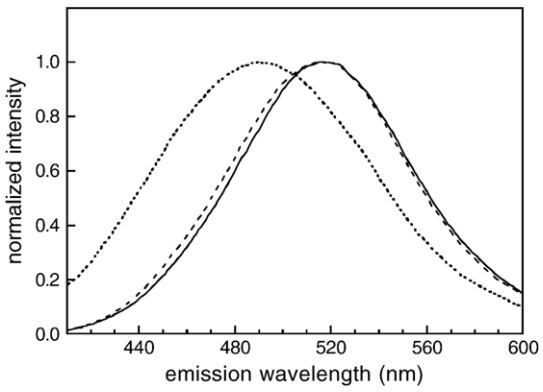

Fig. 1. Fluorescence emission spectrum of $AnxA2^{acryl}$. $AnxA2^{acryl}$ (solid line); $AnxA2^{acryl}$ at pCa3 (dashed line); $AnxA2^{acryl}$ at pCa3, with LUV (PC/PS 75/25) (L/P = 100) (dotted line). Total protein concentration: 0.5 μM in a 120 μL microcuvette. Excitation wavelength 390 nm (slit width 10 nm), emission slit width: 5 nm.

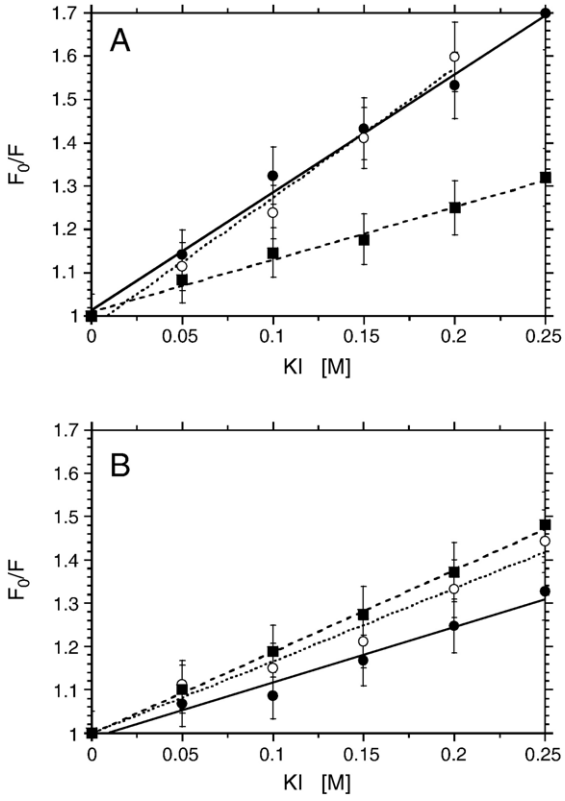

Fig. 2. Stern–Volmer plots of quenching of acrylodan by iodide. A, AnxA2^{acryl}: AnxA2^{acryl} in buffer (●): AnxA2^{acryl} at pCa3 (○); AnxA2^{acryl} LUV L/P=100 at pCa3 (■). B, (AnxA2^{acryl}-p11)$_2$: (AnxA2^{acryl}-p11)$_2$ in buffer (●): (AnxA2^{acryl}-p11)$_2$ at pCa3 (○);(AnxA2^{acryl}-p11)$_2$ LUV L/P=100 at pCa3 (■).

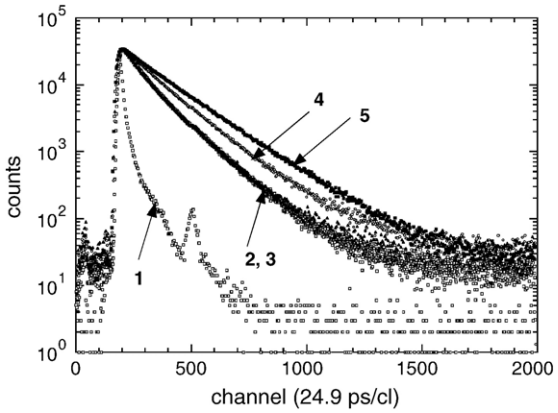

Fig. 3. Time-resolved fluorescence intensity decay of AnxA2^{acryl} and (AnxA2^{acryl}-p11)$_2$. Instrumental response function (curve 1); experimental decays of: AnxA2^{acryl} (curve 2); AnxA2^{acryl} pCa 2.7 (curve 3); AnxA2^{acryl} bound to LUV (PC/PS 75/25) L/P=100 at pCa 2.7 (curve 4); (AnxA2^{acryl}-p11)$_2$ (curve 5). Excitation wavelength: 392 nm, emission wavelength: 505 nm for curves 2, 3 and 480 nm for curves 4, 5. Experimental conditions are shown in the legend to Table 2.

The N-terminal segment displayed rapid dynamics, as monitored by fluorescence anisotropy decay. The experimental anisotropy decay curve decreased rapidly at first, and then more slowly (Fig. 5A). Two time constants were computed: a subnanosecond component and a much longer component with amplitude about twice that of the subnanosecond component (Table 3). The short decay time probably reflects local motion of the acrylodan around its linker. Shorter decay times of small amplitudes, too fast to be measured by the instrumentation, may also have occurred because the anisotropy value at time zero did not reach 0.37, the fundamental anisotropy value measured for completely immobilized acrylodan [48]. These subnanosecond motions were restricted. The semi-angle value of the wobbling-in-cone rotation ω_{max} [49] was large and insensitive to Ca^{2+}. The longest rotational correlation time was consistent with the Brownian rotational motion of a hydrated protein of the size of AnxA2 (Table 3). Its value was similar to that measured from Trp212 fluorescence anisotropy decays [50]. Ca^{2+} had no effect on this parameter.

Table 1
AnxA2^{acryl} and (AnxA2^{acryl}-p11)$_2$ fluorescence quenching by iodide in solution and bound to membrane vesicles (LUV PC/PS 75/25)

Sample	$<\tau>$ (ns)*	K_{SV} (M^{-1})	k_q (nM^{-1})*
AnxA2^{acryl}	1.88	2.73	1.45±0.15
AnxA2^{acryl} pCa3	1.88	2.98	1.59±0.16
AnxA2^{acryl} LUV pCa3	2.15	1.22	0.56±0.06
(AnxA2^{acryl}-p11)2	3.62	1.29	0.36±0.04
(AnxA2^{acryl}-p11)2 pCa3	3.62	1.68	0.46±0.04
(AnxA2^{acryl}-p11)2 LUV pCa3	3.26	1.89	0.58±0.06

Excitation wavelength: 392 nm, emission wavelength: 505 nm for AnxA2^{acryl}, 480 nm for AnxA2^{acryl}-LUV and (AnxA2^{acryl}-p11)$_2$. Protein concentration: 1 μM; L/P=100. Estimated error of± 10%.
*The amplitude average lifetime $<\tau>$ was calculated as $<\tau>=\Sigma\alpha_i\tau_i$ and the bimolecular quenching constant as $k_q=K_{SV}/<\tau>$.

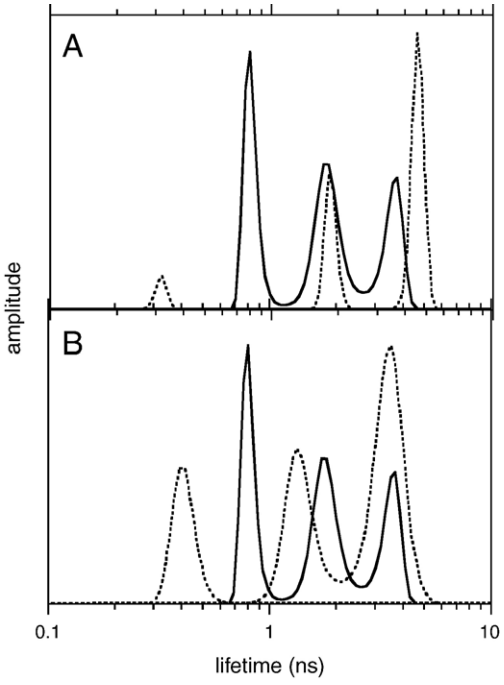

Fig. 4. MEM reconstructed excited state lifetime distribution of AnxA2^{acryl} and (AnxA2^{acryl}-p11)$_2$. A, Solid line: AnxA2^{acryl}; dotted line: (AnxA2^{acryl}-p11)$_2$. B, Solid line: AnxA2^{acryl}; dotted line: AnxA2^{acryl} LUV (PC/PS 75/25) L/P=100 at pCa 2.7. Numerical values are shown in Table 2.

Table 2
MEM recovered excited state lifetime distribution of AnxA2^{acryl} and (AnxA2^{acryl}-p11)$_2$ in buffer and bound to phospholipid vesicles (LUV PC/PS 75/25)

Sample	τ_1 (ns)	τ_2 (ns)	τ_3 (ns)	α_1	α_2	α_3	$<\tau>$ (ns)
AnxA2^{acryl} no calcium	0.60±0.22	1.56±0.43	3.35±0.39	0.27±0.05	0.43±0.03	0.30±0.06	1.84±0.05
AnxA2^{acryl} pCa 2.7	0.54±0.08	1.40±0.06	3.25±0.07	0.21±0.01	0.43±0.02	0.36± 0.02	1.89±0.02
AnxA2^{acryl} LUV pCa4*	0.49±0.11	1.18±0.10	3.31±0.20	0.18±0.03	0.32±0.07	0.50±0.06	2.12±0.15
AnxA2^{acryl} LUV pCa3**	0.48±0.11	1.40±0.07	3.52±0.04	0.23±0.02	0.34±0.01	0.43±0.02	2.10±0.10
(AnxA2^{acryl}-p11)$_2$	0.34±0.12	1.79±0.41	4.51±0.20	0.07±0.03	0.22±0.03	0.71±0.12	3.62±0.16
(AnxA2^{acryl}-p11)$_2$ pCa5	0.26±0.05	1.86±0.02	4.66±0.01	0.09±0.04	0.30±0.01	0.61±0.02	3.42±0.13
(AnxA2^{acryl}-p11)$_2$ pCa3	0.29±0.05	1.78±0.04	4.62±0.01	0.04±0.02	0.34±0.02	0.62±0.01	3.42±0.13
(AnxA2^{acryl}-p11)$_2$ LUV pCa4*	0.80±0.07	2.29±0.28	4.27±0.07	0.14±0.01	0.27±0.01	0.59±0.01	3.26±0.11

Excitation wavelength: 392 nm, emission wavelength: 505 nm for AnxA2^{acryl}, 480 nm for AnxA2^{acryl}-LUV and (AnxA2^{acryl}-p11)$_2$. *L/P=100, **L/P=50; protein concentration: 0.5 μM. The standard deviation values were calculated from 2 to 5 measurements.
Amplitude average lifetime $<\tau>$ is defined as in Table 1.

3.2. Conformational dynamics of the AnxA2 N-terminal segment in the heterotetramer (AnxA2-p11)2 in solution

As observed by Johnsson et al. [21], binding of the p11 dimer to AnxA2 shifted the fluorescence emission spectrum of AnxA2^{acryl} to the blue by about 35 nm (not shown). This confirmed that the fluorophore environment was less polar in (AnxA2^{acryl}-p11)$_2$ than in AnxA2^{acryl}. Consistent with this observation, the quenching efficiency of iodide was lower for the heterotetramer than for AnxA2 alone, as shown by the K_{SV} value (Table 1). The bimolecular quenching constant k_q value, which is the relevant parameter for comparison of solvent accessibilities, calculated from the present lifetime measurements, showed that the accessibility of the fluorophore to the solvent is 3 times lower for the heterotetramer (AnxA2^{acryl}-p11)$_2$ than for the monomer AnxA2^{acryl} (Table 1).

Conformation change of the N-terminal segment is also revealed by the fluorescence intensity decay of the heterotetramer (AnxA2^{acryl}-p11)$_2$ which differed significantly from that of the monomer AnxA2^{acryl} (Fig. 3, curve 5). Overall, acrylodan decay was more homogeneous in the heterotetramer than in the monomer: the lifetime distribution was dominated by a long lifetime of ~5 ns (Fig. 4A and Table 2).

The flexibility of the N-terminal segment, as assessed by fluorescence anisotropy decays, was moreover much lower in (AnxA2^{acryl}-p11)$_2$ than in AnxA2^{acryl}. The experimental fluorescence anisotropy decay curve of (AnxA2^{acryl}-p11)$_2$ included a fast initial component of low amplitude (Fig. 5C) but was dominated by a slow component. The analysis of the data showed 3 time constants: i) one subnanosecond time constant of low amplitude, describing the local rotational motion of the probe around its linker; ii) a nanosecond time constant, probably revealing a

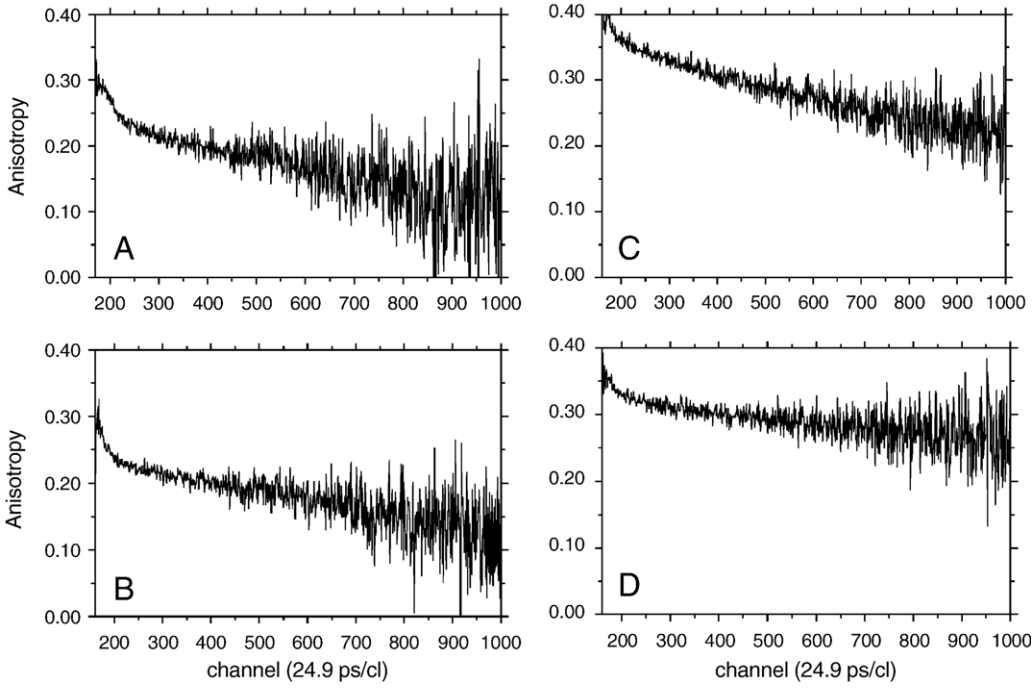

Fig. 5. Experimental fluorescence anisotropy decay of AnxA2^{acryl} and (AnxA2^{acryl}-p11)$_2$. A, AnxA2^{acryl}; B, AnxA2^{acryl} bound to LUV (PC/PS 75/25) (L/P=100, pCa=2.7); C, (AnxA2^{acryl}-p11)$_2$; D, (AnxA2^{acryl}-p11)$_2$ bound to LUV (PC/PS 75/25) (L/P=100, pCa=2.7). Experimental conditions as in Table 2.

Table 3
MEM recovered rotational correlation time distribution AnxA2^{acryl} and (AnxA2^{acryl}-p11)$_2$ in buffer and bound to phospholipid vesicles (LUV PC/PS 75/25)

Sample	β_1	β_2	β_3	θ_1 (ns)	θ_2 (ns)	θ_3 (ns)	$A_{t=0}$	ω_{max}(°)
AnxA2^{acryl}	0.095±0.007	–	0.227±0.005	0.33±0.02	–	26±1	0.322±0.010	32±1
AnxA2^{acryl} pCa 2.7	0.122±0.015	–	0.232±0.003	0.27±0.02	–	25±1	0.354±0.015	31±1
AnxA2^{acryl} LUV pCa4	0.059±0.046	0.118±0.029	0.132±0.035	0.37±0.25	12±5	∞	0.290±0.031	28±3
AnxA2^{acryl} LUV pCa3	0.097±0.011	0.117±0.014	0.148±0.039	0.18±0.06	10±1	∞	0.360±0.035	27±4
(AnxA2^{acryl}-p11)$_2$	0.034±0.019	0.025±0.011	0.336±0.007	0.21±0.04	4.1±0.1	45±3	0.395±0.018	7±5
(AnxA2^{acryl}-p11)$_2$ pCa5	0.007±0.007	0.018±0.006	0.348±0.006	0.13±0.05	2.7±0.1	42±2	0.365±0.020	5±2
(AnxA2^{acryl}-p11)$_2$ pCa3	0.057±0.001	0.080±0.025	0.278±0.029	0.16±0.02	11±3	65±9	0.415±0.015	9±2
(AnxA2^{acryl}-p11)$_2$ LUV pCa4	0.024±0.004	0.083±0.016	0.237±0.019	0.44±0.08	14±3	∞	0.344±0.013	18±5

Experimental conditions as in Table 2.
The θ_i and β_i coefficients are respectively the values of the center and partial anisotropy of each rotational correlation time peak. The semi-angle ω_{max} of the wobbling-in-cone subnanosecond motion was calculated from $(\beta_2+\beta_3)/A_0=[1/2\cos\omega_{max}(1+\cos\omega_{max})]^2$, with $\omega_{max}=\mathrm{Arccos}1/2[(1+8(\Sigma\beta(ns)_i/A_0)^{1/2})^{1/2}-1]$, [49] with the intrinsic anisotropy $A_0=0.370$ measured in vitrified medium [48].

local nanosecond flexibility of the N-terminal segment in the heterotetramer, not present in the monomeric AnxA2 and iii) a long rotational correlation time of high amplitude, corresponding to the Brownian rotational motion of the complex (Table 3), with the same value as that measured from the Trp212 fluorescence anisotropy decay [50]. The semi-angle ω_{max} of the wobbling-in-cone rotation was strongly restricted compared to that in the monomeric AnxA2 (Table 3).

Ca^{2+} in the micromolar concentration range (pCa5) had no major effect on any of the fluorescence characteristics of (AnxA2^{acryl}-p11)$_2$ (Tables 2 and 3). At higher concentrations (pCa3), however, the fluorescence anisotropy decay of (AnxA2^{acryl}-p11)$_2$ showed a significantly higher contribution of nanosecond flexibility (Table 3). The accessibility to the solvent is increased by 20% (Table 1).

3.3. Effect of the interaction of AnxA2 with LUV on the conformational dynamics of the N-terminal segment

One major purpose in this study was to delineate the possible changes of the N-terminal dynamics of the monomeric AnxA2 evoked upon Ca^{2+}-mediated interaction with negatively charged phospholipid membranes. The fluorescence emission parameters of AnxA2^{acryl} were sensitive to these interactions, indicating significant change in the N-terminus conformation and dynamics. These changes were observed whatever the lipidic composition of the membranes (see Materials and methods) and therefore only data obtained with the basic mixture (PC/PS 75/25) are presented.

A large change in the polarity of the fluorophore environment was observed, as inferred from the blue-shift by about 30 nm of its fluorescence emission spectrum induced by membranes in the presence of Ca^{2+}, with respect to the spectrum obtained for AnxA2^{acryl} in solution (Fig. 1). This blue-shift started at pCa ~ 6 and ended at pCa ~ 5 (Fig. 6). It was correlated with the calcium-induced membrane aggregation process, as estimated from turbidity measurements (Fig. 6).

The fluorescence intensity decay of AnxA2^{acryl} bound to LUV was moreover significantly different from that in buffer (Fig. 3, curve 4). A redistribution of the lifetime populations was observed (Fig. 4B): the amplitude of the longest lifetime increased by ~40%, mostly at the expense of the shortest lifetime, resulting in a small increase (~10%) in amplitude-average lifetime (Table 2). This effect probably indicates a change in the relative proportion of acrylodan conformers and therefore a local conformational change of the N-terminal segment. No significant differences were observed between measurements at pCa4 and pCa3 concentrations (Table 2).

As for AnxA2^{acryl} in solution, acrylodan displayed subnanosecond mobility when AnxA2^{acryl} is bound to LUV at aggregative concentrations of Ca^{2+} (Fig. 5B and Table 3). Faster motions probably also occurred, as the initial anisotropy value, $A_{t=0}$, was again lower than that measured in media of high viscosity [48]. The semi-angle ω_{max} of the wobbling-in-cone motion was similar to that of the free protein (Table 3). An infinite time constant was observed, due to the extremely slow rotation of the vesicles on which the protein was bound. Furthermore, a nanosecond rotational correlation time of large amplitude was detected, with values of ~10 ns. This additional flexibility was not observed in the absence of membranes (Table 3). No significant differences were observed between measurements at pCa4 and pCa3 (Table 3).

Consistent with the blue-shift of the fluorescence emission spectrum, indicating a lower polarity of the acrylodan environment in the membrane-bound form of AnxA2 than in the free protein in buffer, iodide quenching was less efficient for the

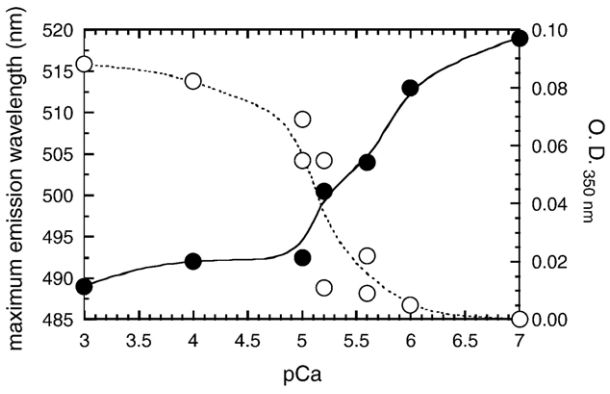

Fig. 6. Correlation between membrane aggregation and fluorescence maxima. Maximum of the fluorescence emission spectrum of AnxA2^{acryl} (●) and turbidity (○) as a function of calcium concentration.

bound form than for the free form as shown by the lower K_{SV} value (Fig. 2 and Table 1). The accessibility of acrylodan to the solvent, as reflected by the k_q value, was lower than for AnxA2 in buffer by a factor of three (Table 1).

3.4. Effect of the interaction of heterotetramer (AnxA2-p11)2 with LUV on the conformational dynamics of the AnxA2 N-terminal segment

The fluorescence emission spectrum of the acrylodan in $(AnxA2^{acryl}\text{-}p11)_2$ bound to LUV (PC/PS 75/25) was not significantly affected compared to the heterotetramer in solution (not shown). Iodide quenching efficiency was increased in LUV compared to the heterotetramer in solution in the presence of Ca^{2+} and the accessibility to the solvent, reflected by the bimolecular quenching constant k_q, increased by ~20% compared to the protein in the presence of Ca^{2+} at pCa3 (Table 1). It did not differ significantly from that in membrane-bound AnxA2 monomer (Table 1).

The excited state lifetime distribution of $(AnxA2^{acryl}\text{-}p11)_2$ bound to LUV differed from that in buffer: the amplitude of the longest lifetime decreased by ~20%, whereas that of the shortest lifetime doubled, leading to a 10% decrease in amplitude-average lifetime (Table 2). These findings are consistent with a slightly higher level of structural heterogeneity or flexibility of the N-terminus in the heterotetramer bound to the membranes.

In agreement with this latter observation, the fluorescence anisotropy decay of $(AnxA2^{acryl}\text{-}p11)_2$ bound to LUV showed an initial fast decay of larger amplitude than in solution (Fig. 5D), corresponding to an increased value of the amplitude of the wobbling-in-cone subnanosecond motion by a factor of two to three (Table 3). The longest rotational correlation time value θ_3 became infinite with respect to the excited state lifetime. Its amplitude was significantly lower than that of the Brownian rotational correlation time for the $(AnxA2^{acryl}\text{-}p11)_2$ in solution (Table 3).

3.5. Location and interactions of the AnxA2 N-terminal segment in Ca^{2+}-bridged membranes

The results presented above show that when monomeric $AnxA2^{acryl}$ binds to LUV, in calcium conditions favouring membrane aggregation, the fluorophore moved to a more hydrophobic environment, more protected from the aqueous solvent than that of the protein in solution.

We may be able to account for these observations by considering direct interactions of the N-terminus with the membrane, as proposed for AnxA1 [4]. To determine the extent of interaction of $AnxA2^{acryl}$ with the membranes, experiments were carried out with LUV (PC/PS 75/25) containing *n*-doxyl PC (distearoyl phosphatidylcholine substituted by a doxyl group bound on the *sn2* acyl chain at 5-, 7- and 12- positions), using the high efficiency of the doxyl group to quench various fluorescence probes at short distances (<10 Å) [51,52]. Whatever the doxyl PC derivative, only weak quenching (15±4%) was observed at a molar fraction of 30% in the LUV, corresponding theoretically to optimal conditions for quenching [53].

Alternatively, protein–protein interactions via the N-termini may occur for the monomeric AnxA2, as recently suggested [32]. For their detection, we performed experiments with AnxA2 molecules with pyrene–maleimide-labelled N-terminal domain, making use of the ability of this probe to form excimers when an excited pyrene moiety diffuses towards a non-excited pyrene moiety during its lifetime [54]. No signature of excimer emission was observed for $AnxA2^{pyr}$ neither in buffer with or without calcium nor in the presence of membranes without calcium (not shown). In contrast, in Ca^{2+}-bridged membranes, in addition to the well resolved vibrational spectrum of the pyrene monomer, we observed a broad-band spectrum characteristic of excimer emission (Fig. 7A), demonstrating interaction between two $AnxA2^{pyr}$ N-terminal segments. The excimer emission spectrum was similar to that observed in similar experiments involving protein–protein interactions [55,56], but was blue-shifted (~460 nm) with respect to the classical spectrum (~480 nm) [57]. This type of spectrum probably results from the formation of "ground-state" excimers [42] when two pyrene rings are separated by short distances (<10 Å), as in an aggregate or a complex. One can also observe that the excimer emission was more intense at 2 °C than at 20 °C (Fig. 7A). In contrary to the monomeric protein, no evidence of excimer formation could be observed for the heterotetramer (Fig. 7B).

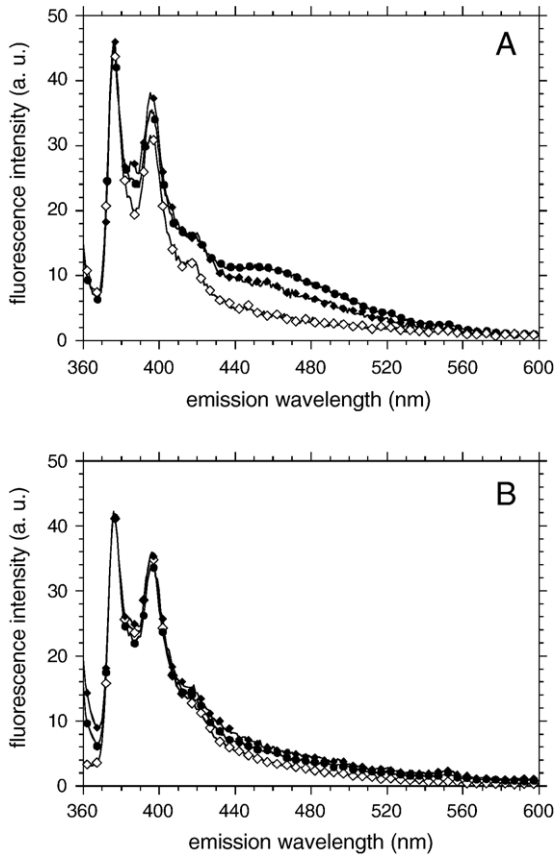

Fig. 7. Fluorescence emission spectrum of $AnxA2^{pyr}$. A: monomeric $AnxA2^{pyr}$; B) heterotetramer $(AnxA2^{pyr}\text{-}p11)_2$. (◊): 0.55 μM protein in buffer at 20 °C; (♦): 0.55 μM protein bound to LUV (PC/PS 75/25) L/P=100 pCa3 at 20 °C; (●): 0.55 μM protein bound to LUV (PC/PS 75/25) L/P=100 pCa3 at 2 °C. Excitation wavelength: 350 nm. Spectra normalized at 378 nm emission.

4. Discussion

In this study, we investigated the microenvironment and dynamics of the N-terminal segment of AnxA2 in various experimental conditions, especially during Ca^{2+}-induced membrane-bridging, by steady-state and time-resolved fluorescence spectroscopy. For this purpose, we labelled the only reactive Cys8 residue in the protein with thiol-reactive fluorescent markers: the polarity-sensitive acrylodan [21] and the excimer-forming probe pyrene–maleimide.

For $AnxA2^{acryl}$ in buffer: i) acrylodan was exposed to a polar environment and therefore highly accessible to the solvent in agreement with Johnsson et al. [21], as shown by its fluorescence emission spectrum and by its quenching by iodide; ii) it was highly mobile in the subnanosecond time range but it did not evidence any nanosecond flexibility of the N-terminus, as shown by fluorescence anisotropy decay and iii) it revealed the existence of conformational heterogeneity, as shown by the heterogeneity of the fluorescence intensity decay. These features were unaffected by the addition of millimolar concentrations of Ca^{2+} which indicates that, in contrast with AnxA1 [58], no Ca^{2+}-induced conformational change occurred for AnxA2 N-terminus.

The absence of nanosecond flexibility in the monomer AnxA2 is of particular importance since nanosecond time constants are signatures of concerted motions of small structured domains or of loops [59,60]. This observation therefore confirms that this sequence is not structured in the full protein in solution, as it has been observed for the isolated N-terminal peptide [21,61]. It remains unstructured in the presence of millimolar concentrations of Ca^{2+}. The absence of an ordered structure for the N-terminal sequence of AnxA2 has also been inferred from the crystal structure of the full-length protein in which the first 20 amino acids were not detected, despite demonstration of the integrity of the protein [36]. Other observations have however indicated that the (1–20) N-terminal segment of AnxA2 displayed the potency to be structured: the sequence encompassing the first 14 amino acids of the N-terminal sequence folded as an amphipathic α-helix, as reported for the 1–28 peptide in a TFE/water mixture [61] and in the complex with p11 [22]. Moreover, a second α-helix encompassing residues P20–A28 was also found in TFE. In AnxA2 in solution, the (1–14) α-helix may account for only a minor fraction of the conformation landscape of the N-terminus and may coexist with dominant less ordered structures exhibiting large flexibility.

In the heterotetramer $(AnxA2^{acryl}\text{-}p11)_2$, the fluorophore was more shielded from the solvent than in $AnxA2^{acryl}$, as shown by the large blue-shift of the fluorescence emission spectrum in agreement with Johnsson et al. [21] and the lower iodide bimolecular quenching constant than that of the $AnxA2^{acryl}$ monomer. The higher homogeneity of the excited-state lifetime distribution and the strong hindrance of the subnanosecond rotational motion of the probe is likely related to the formation of the AnxA2 N-terminal amphipathic α-helix in the heterotetramer, as observed in the crystal structure of the AnxA2 N-terminal (1–14) peptide complexed with the p11 dimer [22]. Acrylodan bound to Cys8 residue being located on the hydrophilic face of the helix, these changes in polarity of its environment and conformation, indicate that this hydrophilic face of the helix participates to the contact surface between the AnxA2 and p11 proteins in the heterotetramer (Fig. 8A). These contact surfaces are flexible in the nanosecond time scale as shown by nanosecond motions observed in the heterotetramer. Micromolar concentrations of Ca^{2+} had no effect on these features. At higher concentrations, Ca^{2+} increased the nanosecond flexibility of these contact surfaces. This last feature was also observed upon interaction of the heterotetramer with the membranes, suggesting that the flexibility of the interface is important to adapt the protein to two fluctuating membrane surfaces (Fig. 8B).

Upon binding of monomeric $AnxA2^{acryl}$ to the negatively charged LUV in the presence of calcium in the submillimolar to millimolar concentration range, where it forms the so-called "homotypic" junctions [39], the microenvironment of the fluorophore became more hydrophobic, as shown by the blue-shift of its steady-state fluorescence emission spectrum. However, this blue-shift was not as large as that expected for an acrylodan-labelled protein deeply embedded in the membrane bilayer [62] or within the hydrophobic core of the protein,

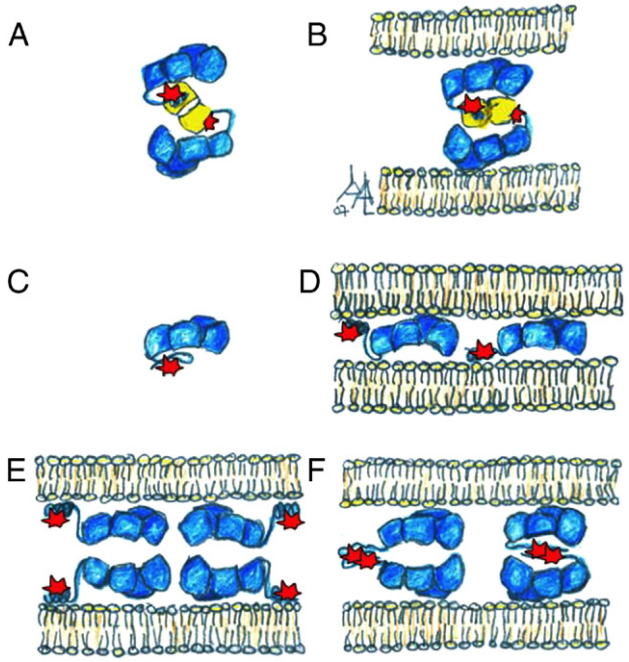

Fig. 8. Schematic topological model for AnxA2 organization in membrane bridges. In solution, the heterotetramer is stabilized by the interaction of S100A10 (in yellow) with the α-helix of the AnxA2 N-terminus (A). In membrane bridges the complex undergoes a subtle conformational change (B) which results in the increase of the AnxA2/p11interface dynamics. The data obtained with fluorescent probes on the Cys8 of the N-terminal tail (red beacon) revealed that the N-terminal domain in an "unfolded" state (C) change to a new conformational state when the protein bridges membranes. D and E show the single protein layer hypothesis and the two layer hypothesis respectively, in which the N-terminal domain lies very close to or in contact with the membrane. Our data disagree with these hypotheses (D) and (E), and support the model (F) in which the protein binds to the membrane via its convex face and protein contacts between the layers are formed at the concave face, allowing N-terminal tail interaction. The two N-terminal domains interact in membrane bridges, and are not in direct contact with the membrane.

where the maximum emission wavelength could be as low as 450 nm [48]. The following fluorescence emission maxima were obtained in pure solvents: 525 nm in water, 460 nm in DMF and 435 nm in dioxane [41]. The fluorescence maximum of ~490 nm obtained for membrane-bound AnxA2^{acryl} in "homotypic" junctions, suggests that acrylodan is located in an environment of intermediate polarity and not deeply embedded in the membrane, whatever the LUV lipid composition. This assumed location is in agreement with the relatively low quenching efficiency of the *n*-doxyl PCs (15% on average for all doxyl positions), even at a high doxyl-PC/lipid molar ratio (30%). Indeed, for proteins or protein domains strongly interacting with membranes, quenching values up to 80% are often observed at this quencher/lipid ratio [63–65]. This low quenching level is likely not due to membrane phase separation of the PC-doxyl quencher for several reasons. First, substitution by a doxyl moiety on a saturated acyl chain confers an unsaturated character to the molecule [66,67]; prone to mix with other unsaturated acyl-chain-bearing phospholipids such as the natural ones we used which contained mixed saturated and polyunsaturated fatty acid chains with low probability of phase separation at the experimental temperature (20 °C). Second, although C5 and C7 derivatives could nevertheless be found in separated gel phases, the C12 derivative was always found in, and even favoured, the liquid disordered phase of phospholipid membranes [66,68]. Third and most important, in these quenching experiments, we used LUV of simple PC/PS composition without cholesterol (absence of liquid ordered phases). We could argue that Ca^{2+}-induced PC/PS phase separation could occur but this has been observed at divalent ion concentrations higher than 1 mM [69,70]. At last, Ca^{2+}-mediated AnxA5 binding to PC/PS membranes occurred without any phase separation between PS and PC in liposome systems at Ca^{2+} concentrations ranging from 0.1 to 1 mM [71,72]. We therefore suggest that the observed weak doxyl-induced quenching of AnxA2^{acryl} in "homotypic" junctions is not due to phase partitioning of the spin-labelled lipid but indicates likely that the AnxA2 N-terminal segment is not in close contact with the membrane/water interface in these membrane models, in agreement with the observation that acrylodan fluorescence emission remains insensitive to the LUV phospholipid composition.

The occurrence of pyrene excimers in AnxA2^{pyr} in "homotypic" junctions clearly demonstrates that N-terminal segment interactions between two AnxA2 molecules can participate to the membrane aggregation process. This interaction is not likely limited by protein diffusion on the membrane surface since lowering the temperature increased the excimer signal. This observed N-terminal contact may account for the disulfide bond-mediated homodimerization involving Cys8 observed after membrane aggregation [32]. The nanosecond motions, revealed by fluorescence anisotropy decays, depict likely the concerted motions of this small structured domain, constituted by two N-terminal segments in interaction. The contact surfaces between the N-termini, which likely stabilize the "homotypic" membrane junctions formed by two AnxA2 monomers, are more flexible than that formed between the AnxA2 N-terminus and p11 in those formed by the heterotetramer. This could in turn explain the relative difficulty to observe these junctions by cryo-electron microscopy, compared to the latter [39]. As it could be reasonably expected from the strong affinity of AnxA2 for the p11 dimer and from the crystal structure of the AnxA2 N-terminal segment with the p11 dimer [22], in which the Cys8 (Ser8) residues are positioned at long distance (~38 angströms), no signature of pyrene excimer formation was detected for the (AnxA2^{pyr}-p11)2 heterotetramer bound to the membrane.

These N-terminal domain interactions in AnxA2 monomer are nevertheless not strictly necessary for Ca^{2+}-induced membrane bridging as the N-terminal deleted protein is able to bridge membranes [28,29]. However, this N-terminal truncated protein needs millimolar calcium concentrations for efficient bridging compared to micromolar calcium concentrations for the complete protein. The N-terminal domains play therefore a crucial role for membrane bridging by AnxA2 monomer, being likely involved in protein–protein interactions at the membrane surface, thereby reducing the required calcium concentration for this process.

In conclusion, these studies show that the formation of "homotypic junctions" [39] by AnxA2 in membrane bridges, in the presence of calcium at neutral pH, involves likely specific interactions between the N-termini of two AnxA2 molecules. Previous reports have suggested that the N-terminus may interact with the membrane bilayer [36], but this assumption was not yet supported by experimental evidences. The present results argue against this possibility (Fig. 8D, E). In contrast, a model can be proposed in which the membrane bridging unit would be constituted by two AnxA2 molecules sandwiched between two membranes, interacting on one side with the membrane surfaces by their convex faces, as it has been previously proposed by Lambert et al. [39] and, on the other side, by their N-termini to stabilize the junction (Fig. 8F). It remains unclear whether the two interacting N-termini remain sandwiched between the concave faces or move to a more lateral position. Lateral interactions between the cores, perhaps of the type described in the crystal structure of Ca^{2+}-bound AnxA2 [36], are nevertheless likely required to account for the continuity of the electron-dense stripes observed on cryo-electron microscopy [39]. Since the N-terminus does not likely interact with phospholipid membranes, the changes in local conformation and dynamics of this domain of the molecule might result from the core domain affecting the N-terminus. Domain III conformation and dynamics in particular is strongly affected by Ca^{2+} and membrane binding [50]. In the cases of AnxA1 and AnxA3 such a relationship has been emphasized [33,34], but it is less clear in the case of AnxA2.

The role of the N-terminal tail dimerization of AnxA2 in the absence of p11 could be of physiological importance depending on the cell type. In cell types in which p11 is expressed at the same (or higher) level than AnxA2, p11 associates with the N-terminal domain of AnxA2 to form the heterotetramer $(AnxA2\text{-}p11)_2$. It is tempting to speculate that in cell types such as adrenergic chromaffin cells in which AnxA2 is expressed in higher quantities than p11 or in cells such as noradrenergic chromaffin cells in which p11 is not expressed, the N-terminal mediated regulation of AnxA2 could increase the efficiency of

Ca^{2+}-induced membrane aggregation and stabilization of membrane bridges.

Acknowledgement

We would like to thank Dr. C. Wolf (INSERM U538, CHU Saint-Antoine, Paris) for kindly providing the *n*-doxyl PC derivatives.

References

[1] V. Gerke, C.E. Creutz, S.E. Moss, Annexins: linking Ca^{2+} signalling to membrane dynamics, Nat. Rev. Mol. Cell Biol. 6 (2005) 449–461.
[2] U. Rescher, V. Gerke, Annexins—unique membrane binding proteins with diverse functions, J. Cell Sci. 117 (2004) 2631–2639.
[3] B.A. Seaton, J.R. Dedman, Annexins, Biometals 11 (1998) 399–404.
[4] V. Gerke, S.E. Moss, Annexins: from structure to function, Physiol. Rev. 82 (2002) 331–371.
[5] S. Liemann, R. Huber, Three-dimensional structure of annexins, Cell. Mol. Life Sci 53 (1997) 516–521.
[6] A. Chander, D.G. Naidu, X.L. Chen, A ten-residue domain (Y11–A20) in the NH2-terminus modulates membrane association of annexin A7, Biochim. Biophys. Acta 1761 (2006) 775–784.
[7] D. Hoekstra, R. Buist-Arkema, K. Klappe, C.P. Reutelingsperger, Interaction of annexins with membranes: the N-terminus as a governing parameter as revealed with a chimeric annexin, Biochemistry 32 (1993) 14194–14202.
[8] W. Wang, C.E. Creutz, Regulation of the chromaffin granule aggregating activity of annexin I by phosphorylation, Biochemistry 31 (1992) 9934–9939.
[9] W. Wang, C.E. Creutz, Role of the amino-terminal domain in regulating interactions of annexin I with membranes: effects of amino-terminal truncation and mutagenesis of the phosphorylation sites, Biochemistry 33 (1994) 275–282.
[10] F. Porte, P. de Santa Barbara, S. Phalipou, J.P. Liautard, J.S. Widada, Change in the N-terminal domain conformation of annexin I that correlates with liposome aggregation is impaired by Ser-27 to Glu mutation that mimics phosphorylation, Biochim. Biophys. Acta 1293 (1996) 177–184.
[11] M. de la Fuente, A.V. Parra, Vesicle aggregation by annexin I: role of a secondary membrane binding site, Biochemistry 34 (1995) 10393–10399.
[12] E. Bitto, M. Li, A.M. Tikhonov, M.L. Schlossman, W. Cho, Mechanism of annexin I-mediated membrane aggregation, Biochemistry 39 (2000) 13469–13477.
[13] K.L. Gould, J.R. Woodgett, C.M. Isacke, T. Hunter, The protein–tyrosine kinase substrate p36 is also a substrate for protein kinase C in vitro and in vivo, Mol. Cell. Biol 6 (1986) 2738–2744.
[14] S.A. Johnstone, I. Hubaishy, D.M. Waisman, Phosphorylation of annexin II tetramer by protein kinase C inhibits aggregation of lipid vesicles by the protein, J. Biol. Chem. 267 (1992) 25976–25981.
[15] M. Jost, V. Gerke, Mapping of a regulatory important site for protein kinase C phosphorylation in the N-terminal domain of annexin II, Biochim. Biophys. Acta 1313 (1996) 283–289.
[16] T. Becker, K. Weber, N. Johnsson, Protein–protein recognition via short amphiphilic helices; a mutational analysis of the binding site of annexin II for p11, EMBO J. 9 (1990) 4207–4213.
[17] D.M. Sullivan, N.B. Wehr, M.M. Fergusson, R.L. Levine, T. Finkel, Identification of oxidant-sensitive proteins: TNF-alpha induces protein glutathiolation, Biochemistry 39 (2000) 11121–11128.
[18] D.A. Eberhard, L.R. Karns, S.R. VandenBerg, C.E. Creutz, Control of the nuclear-cytoplasmic partitioning of annexin II by a nuclear export signal and by p11 binding, J. Cell Sci. 114 (2001) 3155–3166.
[19] J. Liu, C.A. Rothermund, J. Ayala-Sanmartin, J.K. Vishwanatha, Nuclear annexin II negatively regulates growth of LNCaP cells and substitution of ser 11 and 25 to glu prevents nucleo-cytoplasmic shuttling of annexin II, BMC Biochem. 4 (2003) 10.
[20] N. Johnsson, J. Vandekerckhove, J. Van Damme, K. Weber, Binding sites for calcium, lipid and p11 on p36, the substrate of retroviral tyrosine-specific protein kinases, FEBS Lett. 198 (1986) 361–364.
[21] N. Johnsson, G. Marriott, K. Weber, p36, the major cytoplasmic substrate of src tyrosine protein kinase, binds to its p11 regulatory subunit via a short amino-terminal amphiphatic helix, EMBO J. 7 (1988) 2435–2442.
[22] S. Rety, J. Sopkova, M. Renouard, D. Osterloh, V. Gerke, S. Tabaries, F. Russo-Marie, A. Lewit-Bentley, The crystal structure of a complex of p11 with the annexin II N-terminal peptide, Nat. Struct. Biol. 6 (1999) 89–95.
[23] J.R. Glenney, Jr., M. Boudreau, R. Galyean, T. Hunter, B. Tack, Association of the S-100-related calpactin I light chain with the NH2-terminal tail of the 36-kDa heavy chain, J. Biol. Chem. 261 (1986) 10485–10488.
[24] S. Rety, D. Osterloh, J.P. Arie, S. Tabaries, J. Seeman, F. Russo-Marie, V. Gerke, A. Lewit-Bentley, Structural basis of the Ca^{2+}-dependent association between S100C (S100A11) and its target, the N-terminal part of annexin I, Structure 8 (2000) 175–184.
[25] T. Sudo, H. Hidaka, Regulation of calcyclin (S100A6) binding by alternative splicing in the N-terminal regulatory domain of annexin XI isoforms, J. Biol. Chem. 273 (1998) 6351–6357.
[26] M. Watanabe, Y. Ando, H. Tokumitsu, H. Hidaka, Binding site of annexin XI on the calcyclin molecule, Biochem. Biophys. Res. Comm. 196 (1993) 1376–13282.
[27] S. De Seranno, C. Benaud, N. Assard, S. Khediri, V. Gerke, J. Baudier, C. Delphin, Identification of an AHNAK binding motif specific for the Annexin2/S100A10 tetramer, J. Biol. Chem. 281 (2006) 35030–35038.
[28] J. Ayala-Sanmartin, P. Gouache, J.P. Henry, N-Terminal domain of annexin 2 regulates Ca^{2+}-dependent membrane aggregation by the core domain: a site directed mutagenesis study, Biochemistry 39 (2000) 15190–15198.
[29] J. Ayala–Sanmartin, Cholesterol enhances phospholipid binding and aggregation of annexins by their core domain, Biochem. Biophys. Res. Comm. 283 (2001) 72–79.
[30] D.S. Drust, C.E. Creutz, Aggregation of chromaffin granules by calpactin at micromolar levels of calcium, Nature 331 (1988) 88–91.
[31] K. Monastyrskaya, E.B. Babiychuk, A. Hostettler, U. Rescher, A. Draeger, Annexins as intracellular calcium sensors, Cell Calcium 41 (2006) 207–219.
[32] J. Ayala-Sanmartin, N. Cavusoglu, J. Masliah, G. Trugnan, Homodimerization of Annexin 2. Role of the N-terminal tail and modulation of membrane aggregation properties, Annexins 1 (2004) 19–25.
[33] B. Favier-Perron, A. Lewit-Bentley, F. Russo-Marie, The high-resolution crystal structure of human annexin III shows subtle differences with annexin V, Biochemistry 35 (1996) 1740–1744.
[34] A. Rosengarth, V. Gerke, H. Luecke, X-ray structure of full-length annexin 1 and implications for membrane aggregation, J. Mol. Biol. 306 (2001) 489–498.
[35] J.T. Tran, A. Rosengarth, H. Luecke, Cloning, purification and crystallization of full-length human annexin 2, Acta Crystallogr., D Biol. Crystallogr. 58 (2002) 1854–1857.
[36] A. Rosengarth, H. Luecke, Annexin A2. Does it induce membrane aggregation by a new multimeric state of the protein, Annexins 1 (2004) 129–136.
[37] N. Johnsson, K. Johnsson, K. Weber, A discontinuous epitope on p36, the major substrate of src tyrosine–protein-kinase, brings the phosphorylation site into the neighbourhood of a consensus sequence for Ca^{2+}/lipid-binding proteins, FEBS Lett. 236 (1988) 201–204.
[38] C. Thiel, K. Weber, V. Gerke, Characterization of a discontinuous epitope on annexin II by site-directed mutagenesis, FEBS Lett 285 (1991) 59–62.
[39] O. Lambert, V. Gerke, M.F. Bader, F. Porte, A. Brisson, Structural analysis of junctions formed between lipid membranes and several annexins by cryo-electron microscopy, J. Mol. Biol. 272 (1997) 42–55.
[40] G. Weber, F.J. Farris, Synthesis and spectral properties of a hydrophobic fluorescent probe: 6-propionyl-2-(dimethylamino)naphthalene, Biochemistry 18 (1979) 3075–3078.
[41] F.G. Prendergast, M. Meyer, G.L. Carlson, S. Iida, J.D. Potter, Synthesis, spectral properties, and use of 6-acryloyl-2-dimethylaminonaphthalene (Acrylodan). A thiol-selective polarity-sensitive fluorescent probe, J. Biol. Chem. 258 (1983) 7541–7544.
[42] F.M. Winnik, Photophysics of preassociated pyrenes in aqueous polymer solutions and in other organized media, Chem. Rev. 93 (1993) 587–614.

[43] M. Baez, P.H. Rodriguez, J. Babul, V. Guixe, Structural and functional roles of Cys-238 and Cys-295 in *Escherichia coli* phosphofructokinase-2, Biochem. J. 376 (2003) 277–283.
[44] J. Ayala–Sanmartin, J.P. Henry, L.A. Pradel, Cholesterol regulates membrane binding and aggregation by annexin 2 at submicromolar Ca^{2+} concentration, Biochim. Biophys. Acta 1510 (2001) 18–28.
[45] A.K. Livesey, J.C. Brochon, Analyzing the distribution of decay constants in pulse-fluorimetry using the maximum entropy method, Biophys. J. 52 (1987) 693–706.
[46] M. Vincent, J.C. Brochon, F. Merola, W. Jordi, J. Gallay, Nanosecond dynamics of horse heart apocytochrome *c* in aqueous solution as studied by time-resolved fluorescence of the single tryptophan residue (Trp-59), Biochemistry 27 (1988) 8752–8761.
[47] M. Vincent, J. Gallay, The interactions of horse heart apocytochrome *c* with phospholipid vesicles and surfactant micelles: time-resolved fluorescence study of the single tryptophan residue (Trp-59), Eur. Biophys. J. 20 (1991) 183–191.
[48] J. Gallay, M. Vincent, I.M. Li De La Sierra, H. Munier-Lehmann, M. Renouard, H. Sakamoto, O. Barzu, A.M. Gilles, Insight into the activation mechanism of *Bordetella pertussis* adenylate cyclase by calmodulin using fluorescence spectroscopy, Eur. J. Biochem. 271 (2004) 821–833.
[49] K.J. Kinosita, S. Kawato, A. Ikegami, A theory of fluorescence polarization decay in membranes, Biophys. J. 20 (1977) 289–305.
[50] J. Ayala-Sanmartin, M. Vincent, J. Sopkova, J. Gallay, Modulation by Ca^{2+} and membrane binding of the structure and dynamics of domain III of AxII (p36) and axII-p11 complex (p90): implications in biochemical properties, Biochemistry 39 (2000) 15179–15189.
[51] E. London, G.W. Feigenson, Fluorescence quenching in model membranes. 1. Characterization of quenching caused by a spin-labeled phospholipid, Biochemistry 20 (1981) 1932–1938.
[52] A. Chattopadhyay, E. London, Parallax method for direct measurement of membrane penetration depth utilizing fluorescence quenching by spin-labeled phospholipids, Biochemistry 26 (1987) 39–45.
[53] A.S. Ladokhin, Analysis of protein and peptide penetration into membranes by depth-dependent fluorescence quenching: theoretical considerations, Biophys. J. 76 (1999) 946–955.
[54] H.J. Galla, W. Hartmann, Excimer-forming lipids in membrane research, Chem. Phys. Lipids 27 (1980) 199–219.
[55] K. Jung, H. Jung, J. Wu, G.G. Prive, H.R. Kaback, Use of site-directed fluorescence labeling to study proximity relationships in the lactose permease of *Escherichia coli*, Biochemistry 32 (1993) 12273–12278.
[56] P. Hammarstrom, M. Persson, P.O. Freskgard, L.G. Martensson, D. Andersson, B.H. Jonsson, U. Carlsson, Structural mapping of an aggregation nucleation site in a molten globule intermediate, J. Biol. Chem. 274 (1999) 32897–32903.
[57] J.B. Birks, Photophysics of Aromatic Molecules, Wiley-Interscience, John Wiley & Sons, Ltd, London, 1970.
[58] A. Rosengarth, H. Luecke, A calcium-driven conformational switch of the N-terminal and core domains of annexin A1, J. Mol. Biol. 326 (2003) 1317–1325.
[59] T. Ichiye, M. Karplus, Fluorescence depolarization of tryptophan residues in proteins: a molecular dynamics study, Biochemistry 22 (1983) 2884–2893.
[60] G.F. Schroder, U. Alexiev, H. Grubmuller, Simulation of fluorescence anisotropy experiments: probing protein dynamics, Biophys. J. 89 (2005) 3757–3570.
[61] Y.H. Hong, H.S. Won, H.C. Ahn, B.J. Lee, Structural elucidation of the protein- and membrane-binding properties of the N-terminal tail domain of human annexin II, J. Biochem. (Tokyo) 134 (2003) 427–432.
[62] A. Valeva, I. Walev, F. Boukhallouk, T.M. Wassenaar, N. Heinz, J. Hedderich, S. Lautwein, M. Mocking, S. Weis, A. Zitzer, S. Bhakdi, Identification of the membrane penetrating domain of *Vibrio cholerae* cytolysin as a beta-barrel structure, Mol. Microbiol. 57 (2005) 124–131.
[63] A. Cruz, C. Casals, I. Plasencia, D. Marsh, J. Perez-Gil, Depth profiles of pulmonary surfactant protein B in phosphatidylcholine bilayers studied by fluorescence and electron spin resonance spectroscopy, Biochemistry 37 (1998) 9488–9496.
[64] X. Chen, D.E. Wolfgang, N.S. Sampson, Use of the parallax-quench method to determine the position of the active-site loop of cholesterol oxidase in lipid bilayers, Biochemistry 39 (2000) 13383–13389.
[65] S.M. Raja, S.S. Rawat, A. Chattopadhyay, A.K. Lala, Localization and environment of tryptophans in soluble and membrane-bound states of a pore-forming toxin from *Staphylococcus aureus*, Biophys. J. 76 (1999) 1469–1479.
[66] S.C. Chen, B.J. Gaffney, Paramagnetic resonance evidence for phase transitions in bilayers of pure spin-labeled lipids, J. Magn. Reson. 29 (1978) 341–353.
[67] S.C. Chen, J.M. Sturtevant, K. Conklin, B.J. Gaffney, Calorimetric evidence for phase transitions in spin-label lipid bilayers, Biochemistry 21 (1982) 5096–5101.
[68] S.N. Ahmed, D.A. Brown, E. London, On the origin of sphingolipid/cholesterol-rich detergent-insoluble cell membranes: physiological concentrations of cholesterol and sphingolipid induce formation of a detergent-insoluble, liquid-ordered lipid phase in model membranes, Biochemistry 36 (1997) 10944–10953.
[69] D. Hoekstra, Fluorescence method for measuring the kinetics of Ca^{2+}-induced phase separations in phosphatidylserine-containing lipid vesicles, Biochemistry 21 (1982) 1055–1061.
[70] J.R. Silvius, Calcium-induced lipid phase separations and interactions of phosphatidylcholine/anionic phospholipid vesicles. Fluorescence studies using carbazole-labeled and brominated phospholipids, Biochemistry 29 (1990) 2930–2938.
[71] P. Meers, D. Daleke, K. Hong, D. Papahadjopoulos, Interactions of annexins with membrane phospholipids, Biochemistry 30 (1991) 2903–2908.
[72] O. Saurel, L. Cézanne, A. Milon, J.F. Tocanne, P. Demange, Influence of annexin V on the structure and dynamics of phosphatidylcholine/phosphatidylserine bilayers: a fluorescence and NMR study, Biochemistry 37 (1998) 1403–1410.